2015

Deposition Thickness Modeling and Parameter Identification for Spray Assisted Vacuum Filtration Process in Additive Manufacturing

August Mark
University of Central Florida

DEPOSITION THICKNESS MODELING AND PARAMETER IDENTIFICATION FOR SPRAY ASSISTED VACUUM FILTRATION PROCESS IN ADDITIVE MANUFACTURING

by

AUGUST MARK
B.S. University of Central Florida, 2013

A thesis submitted in partial fulfillment of the requirements
for the degree of Master of Science
in the Department of Mechanical and Aerospace Engineering
in the College of Engineering and Computer Science
at the University of Central Florida
Orlando, Florida

Fall Term
2015

Major Professor:
Yunjun Xu

ABSTRACT

To enhance mechanical and/or electrical properties of composite materials used in additive manufacturing, nanoparticles are often time deposited to form nanocomposite layers. To customize the mechanical and/or electrical properties, the thickness of such nanocomposite layers must be precisely controlled. A thickness model of filter cakes created through a spray assisted vacuum filtration is presented in this paper, to enable the development of advanced thickness controllers. The mass transfer dynamics in the spray atomization and vacuum filtration are studied for the mass of solid particles and mass of water in differential areas, and then the thickness of a filter cake is derived. A two-loop nonlinear constrained optimization approach is used to identify the unknown parameters in the model. Experiments involving depositing carbon nanofibers in a sheet of paper are used to measure the ability of the model to mimic the filtration process.

ACKNOWLEDGMENTS

I would like to thank Dr. Yunjun Xu for his constant help and advice.

I would also like to thank the rest of the faculty and staff at University of Central Florida for their instruction and the engineering skills they have passed on to me.

I would also like to thank Dr. Jihua Gou and Dr. Kurt Lin for being on my thesis committee and advising me during this research.

I would like to thank John Sparkman for his technical knowledge and for helping with the identification experiments.

I would like to thank my friends and family for their constant support during my time in graduate school.

TABLE OF CONTENTS

LIST OF FIGURES

LIST OF TABLES

CHAPTER 1

INTRODUCTION

1.1 Nanocomposite Structures

Due to their desirable mechanical, electrical, and thermal properties when compared to traditional materials, composite materials enjoy a wide range of applications, and see use in the automotive [1], aerospace [2], and renewable energy industries [3]. Nanocomposite structures are of particular interest due to the unique material properties that can be achieved by mixing particular nanoparticle filler materials with composite structures. For example, carbon nanotubes and graphene are also frequently selected due to their high mechanical strength and electrical conductivity, and are frequently used in sensors, solar cells, and electromagnetic interference shielding [4].

Several methods for creating nanocomposite structures exist. In the melt process, a polymer is heated until it is melted, and is then mixed with filler materials [4]. In the sol-gel method, an organic polymer gel and a precipitate of filler materials are mixed together for 1 hour, left to digest for several hours, rinsed, dewatered, ground up, treated with an acid solution, and rinsed and dewatered one last time [5]. However, these methods are not

without their drawbacks. In the melt process, the high viscosity of the melted polymer limits the dispersion of the filler material [4]. The sol-gel method is very time consumptive, and requires several steps and many pieces of equipment to carry out [5].

1.2 Spray Assisted Vacuum Filtration

Simple nanocomposite structures can be quickly created by adding layers of nanoparticles to a resin. One method commonly used to make these layers is vacuum filtration. Vacuum filtration is a process by which the liquid in a solid-liquid mixture is forced through a filter medium that the solid cannot pass through using vacuum pressure [6]. However, applying vacuum filtration to a suspended solid-liquid mixture cannot create nanoparticle layers with controllable thickness profiles, as the amount of liquid removed in vacuum filtration is related to the liquid content in the suspended mixture. Taking inspiration from spray coating methods used in additive manufacturing, it is noted that if controlled amounts of a solid-liquid mixture are only added to specific areas on a filter medium over time, then the liquid volume content of the suspended mixture can be controlled, yielding nanoparticle layers with controllable thickness profiles.

Spray coating has been widely used in decorative painting [7], thermal barriers [8], and solar cells [9]. Several different types of spray coating exist, including direct spray [10], electrospray [11], and thermal spray [12]. In direct spray in particular, a solution or mixture is atomized, and the resulting droplets are applied to a surface. By controlling the motion

of the spray applicator used, direct spray can be used to distribute a mixture onto a surface, adding only specific amounts of mixture where desired.

The dynamic processes from spray coating and vacuum filtration can be combined to create a thickness model for spray assisted vacuum filtration. This model is expected to be used later to design controllers that can precisely control the thickness of nanoparticle layers created using this additive manufacturing process. This kind of precision control is necessary for customizing the material properties of nanocomposites made with nanoparticle layers. For example, increasing the thickness of graphene layers increases their electrical and thermal conductivity, and varying the thickness of these graphene layers can create more uniform heat and current flux profiles within a nanocomposite structure, as the conductivity of these structures is dependent on their morphology [13].

1.3 Thesis Outline

Chapter two uses the mass transfer dynamics from spray atomization and vacuum filtration to develop differential equations for the solid mass, water mass, and thickness of filter cakes. Chapter three presents a model validation experiment, as well as a discussion on how to estimate the unknown terms present in the model by using a nested loop of two nonlinear constrained optimizations.

Chapter four provides a short conclusion on the findings of this thesis.

1.4 Contribution of Thesis

While spray assisted vacuum filtration has been used before, no process model has been developed to quantitatively measure the mass and thickness change of the achieved layers. Additionally, this model is expressed in a state space form, which is expedient for those wishing to use the model to derive advanced controllers to precisely control the mass, mass distribution, and thickness of nanoparticle layers. The trajectory planning problem has already been discussed for the spray coating process. A frequency domain approach has been used to determine the optimal path to create uniform coverage of a flat area [14]. A similar approach can be taken for the trajectory planning problem for spray assisted vacuum filtration. The composition of the nanoparticles dramatically impacts the mechanical and electrical properties of the manufactured products [15].

CHAPTER 2

PROCESS MODELING

Spray assisted vacuum filtration is an additive manufacturing process which uses spray atomization and vacuum filtration to create cakes of solid particulate. Spray atomization is the process by which a bulk solution or mixture is turned into a dispersion of droplets [16]. This is typically done by using a gage pressure to force a solution through an atomizing nozzle [16]. Vacuum filtration is the process by which a liquid is separated from a solid-liquid mixture by using vacuum pressure to force the liquid through a medium the solid cannot pass through [6].

The mass transfer dynamics in both the spray atomization and the vacuum filtration steps are discussed. Via these two dynamics, the thickness model of the nanoparticle layer is derived.

2.1 Spray Modeling

A mixture of water and solid particles are deposited via the means of spray application. As shown in [14], the mass deposited onto a differential area dA for a given amount of time is

$$dm_d = \int_{t_0}^{t_f} \dot{m}_s \Theta dA dt \tag{2.1.1}$$

Here dm_d is the mass deposited onto a differential area, $\dot{m}_s$ is the total rate of mass transfer from a spray applicator, Θ is the distribution of droplets within the spray and has the unit $\frac{1}{m^2}$, t_0 is the starting time, and t_f is the final time. In this paper, an airbrush, typical to what is used in painting, is used to deposit material. From [16], this type of spray applicator can be considered an air-assist atomizer, and $\dot{m}_s$ can be modeled as

$$\dot{m}_s = C_D A_s \sqrt{2\rho_s \Delta P_s} \tag{2.1.2}$$

Here, C_D is the discharge coefficient, A_s is the area of the spray applicator at its outlet, ρ_s is the density of fluid within the spray applicator, and ΔP_s is the gage pressure applied to the spray applicator. C_D is dependent on factors including the Reynolds Number inside the nozzle of the spray applicator, the length to diameter ratio of the nozzle, the pressure applied to the nozzle, the ambient gas pressure, the presence of an inlet chamfer, and the presence of any cavitation within the nozzle [16]. These values are difficult to estimate; for the time being C_D is left unknown and will be identified later.

Several different models for Θ exist. Θ can be constant [17], a regularized Dirac function [14], a Gaussian distribution [18] or a symmetric quartic function [19]. For simplicity, this paper assumes Θ is constant over a circular area, and can be given as

$$\Theta = H(\gamma - \theta)/(\pi z_a^2 tan^2\gamma) \tag{2.1.3}$$

As shown in Figure 2.1, z_a is the height of the nozzle outlet above the sprayed area, γ is the maximum spray angle, and θ is a step function defined as $H(x) = 0$ for all $x \leq 0$ and $H(x) = 1$ for all $x > 0$. An important note is that that integrating Θ over the entire sprayed area results in unity.

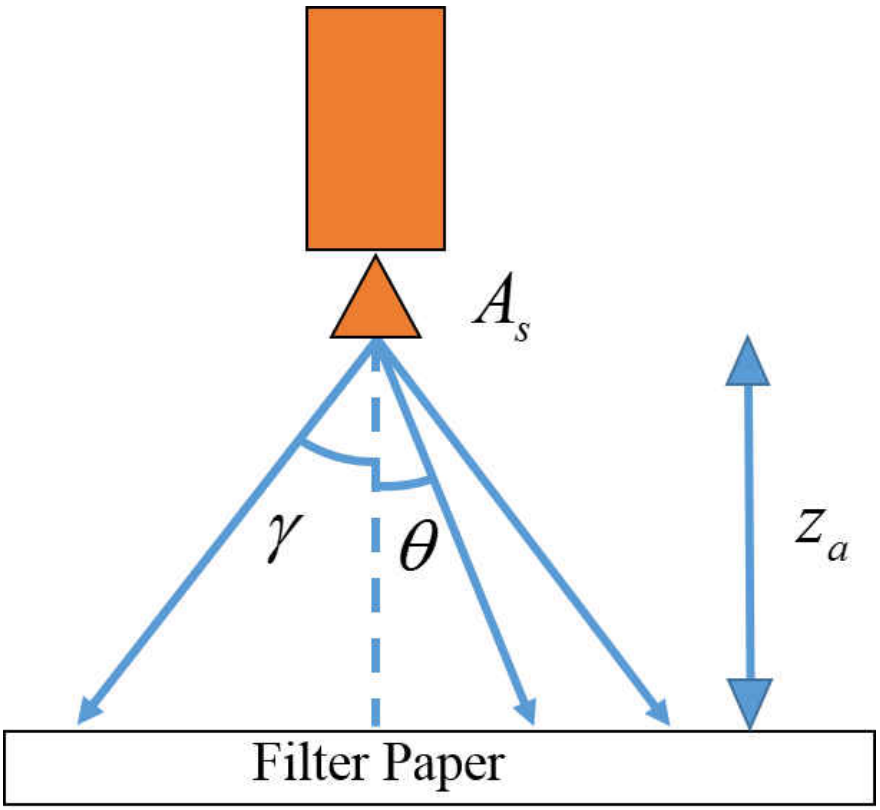

Figure 2.1: Spray Visualization

The mass sprayed onto the differential area can then be found by substituting Equations (2.1.2) and (2.1.3) into Equation (2.1.1) as

$$dm_d = \int_{t_0}^{t_f} \frac{C_D A_s \sqrt{2\rho_s \Delta P_s} dA}{\pi z_a^2 tan^2 \gamma} H(\gamma - \theta) dt \tag{2.1.4}$$

For simplicity, several of the known constant terms in Equation (2.1.4) can be grouped into a constant C_I. Equation (2.1.4) can then be rewritten as

$$dm_d = \int_{t_0}^{t_f} C_D C_I dA H(\gamma - \theta) dt \tag{2.1.5}$$

$$C_I = \frac{A_s \sqrt{2\rho_s \Delta P_s}}{\pi z_a^2 tan^2 \gamma} \tag{2.1.6}$$

2.2 Vacuum Filtration Modeling

Within dm_d, the solid particle mass dm_p deposited onto a differential area can be given by

$$dm_p = s dm_d = c \rho_p \delta dA \tag{2.2.1}$$

Here s is the mass fraction of the solid particles with respect to the sprayed solution. c is the volume fraction of the solid particles with respect to the filter cake within the differential area dA. ρ_p is the density of the solid particles, and δ is the thickness of the filter cake at a given time.

Since the mixture in the spray only contains water and solid particles, and the filter cake also only contains water and solid particles, the mass fraction of the water within the

sprayed mixture is $(1-s)$, and the volume fraction of the water within the filter cake within a differential area dA is $(1-c)$. The water mass dm_w deposited onto a differential area can be given by

$$dm_w = (1-s)dm_d - dm_f = (1-c)\rho_w \delta dA \tag{2.2.2}$$

Here dm_f is the mass of the water which has been filtered out from this differential area, and ρ_w is the density of water. The filtered water dm_f can be derived from Darcys Law. In its most basic form, Darcys Law describes the flow of a liquid through a filter due to an applied pressure [6] as

$$\frac{\Delta P}{L_F} = \frac{\mu q}{k_F A} \tag{2.2.3}$$

Here ΔP is the pressure applied to the filter, i.e. the pressure between the top and bottom surface of the filter, L_F is the thickness of the filter, μ is the viscosity of the liquid passing through the filter, q is the liquid volume flow rate through the filter, k_F is the porosity of the filter, and A is the surface area of the filter. Typically, the liquid must pass through both the filter medium and a growing filter cake, both of which add resistance to filtration. Equation (2.2.3) can then be expanded to reflect that the liquid must pass through both mediums [6].

$$\Delta P = \frac{\mu q}{A}\left[\frac{L}{k} + \frac{L_F}{k_F}\right] \tag{2.2.4}$$

Here L is the uniform thickness of the filter cake and k is the permeability of the filter cake. The terms L_F and k_F are both constant, and can be lumped together and treated as the filter resistance R_F. Unfortunately, the manufacturer supplied information frequently does not provide a convenient value for R_F. Instead, a water volume flux rate is provided. If R_F is substituted into Equation (2.2.4) and L is set equal to 0, an expression can be found for R_F.

$$R_F = \frac{L_F}{k_F} = \frac{\Delta P}{\mu}\frac{A}{q} = C_F\frac{\Delta P}{\mu} \tag{2.2.5}$$

Here, C_F, a filter resistance constant, is the inverse of the water volume flux flow rate. However, the conditions under which C_F is found in the manufacturer supplied information are unknown, and could potentially vary from what is observed in this model. As a result, C_F is left unknown and will be identified later.

Equation (2.2.4) can be modified to examine only the volume of water filtered out in a small differential area dA by replacing A with dA, L with δ, μ with μ_w, and q with dq. From [6], it is known that the vacuum pressure applied is constant across the entire filter cake throughout vacuum filtration. Equation (2.2.4) can then be solved for dq, and Equation (2.2.5) can be substituted in for L_F and k_F.

$$\Delta P = \frac{\mu_w dq}{dA}\left[\frac{\delta}{k} + \frac{L_F}{k_F}\right] \tag{2.2.6}$$

$$dq = \frac{\Delta P dA}{\mu} \left[\frac{\delta}{k} + C_F \frac{\Delta P}{\mu_w} \right]^{-1} \tag{2.2.7}$$

dm_f can now be calculated by multiplying Equation (2.2.7) by ρ_w and taking a time integral of both sides.

$$dm_f = \int_{t_0}^{t_f} \rho_w dq \; dt \tag{2.2.8}$$

$$dm_f = \frac{\rho_w \Delta P dA}{\mu} \int_{t_0}^{t_f} \left[\frac{\delta}{k} + C_F \frac{\Delta P}{\mu_w} \right]^{-1} \; dt \tag{2.2.9}$$

The permeability of the filter cake, k, changes over time with the composition of the filter cake, with more concentrated filter cakes having less permeability [6]. Power laws can be used to relate c and the specific resistance to filtration, represented as α, to the initial gage pressure applied to the filter cake, $P_{c,0}$, and the change in gage pressure applied to the filter cake, ΔP_c [6]. These power laws are repeated below.

$$c = c_0 \left[1 + \frac{\Delta P_c}{P_{c,0}} \right]^u \tag{2.2.10}$$

$$\alpha = \alpha_0 \left[1 + \frac{\Delta P_c}{P_{c,0}} \right]^n \tag{2.2.11}$$

$$\alpha = \frac{1}{kc\rho_p} \tag{2.2.12}$$

Here, c_0 is the initial concentration, α_0 is the initial specific resistance to filtration, and u and n are unknown, experimentally determined constants. A power law relation can be found between c and k by combining Equations (2.2.10), (2.2.11), and (2.2.12). First, solve Equation (2.2.12) for k.

$$k = \frac{1}{\alpha c \rho_p} \tag{2.2.13}$$

Note that k_0, the initial permeability, can be found by substituting α_0 and c_0 into Equation (2.2.13).

$$k_0 = \frac{1}{\alpha_0 c_0 \rho_p} \tag{2.2.14}$$

Now, substitute Equations (2.2.10) and (2.2.11) into Equation (2.2.13), and use Equation (2.2.14) to combine the constant terms.

$$k = (\alpha_0 c_0 \rho_p \left[1 + \frac{\Delta P_c}{P_{c,0}}\right]^{n+u})^{-1} \tag{2.2.15}$$

$$k = k_0 \left[1 + \frac{\Delta P_c}{P_{c,0}}\right]^{-n-u} \tag{2.2.16}$$

Now, solve for the pressure terms in Equation (2.2.10), and raise both sides to the power $(-n/u - 1)$.

$$\frac{c}{c_0} = \left[1 + \frac{\Delta P_c}{P_{c,0}}\right]^u \tag{2.2.17}$$

$$\frac{c}{c_0}^{-n/u-1} = \left[1 + \frac{\Delta P_c}{P_{c,0}}\right]^{-n-u} \tag{2.2.18}$$

Finally, substitute Equation (2.2.18) into Equation (2.2.16).

$$k = k_0 \frac{c}{c_0}^{-n/u-1} \tag{2.2.19}$$

$$k = C_k c^{-1-\tau} \tag{2.2.20}$$

Here, τ is the combination of u and n in Equation (2.2.19), and C_k is the combination of k_0 and c_0 in Equation (2.2.19). For the time being, τ and C_k are left as unknowns, and will be identified later. To get Equation (2.2.20) in terms of dm_p, dm_w, and δ, either Equation (2.2.1) or (2.2.2) can be used to solve for c. The rest of this paper leaves c ambiguous.

2.3 Process Modeling

Equations (2.1.5) through (2.2.20) can now be used to derive expressions for the time derivatives of dm_p, dm_w, and δ. To find $\dot{dm_p}$, combine Equations (2.1.5) and (2.2.1) and take a time derivative.

$$dm_p = s \int_{t_0}^{t_f} C_D C_I dAH(\gamma - \theta) dt \tag{2.3.1}$$

$$d\dot{m}_p = sC_D C_I dAH(\gamma - \theta) \tag{2.3.2}$$

The increase rate of the solid particle mass due to the spray process is constant as long as the differential area dA is within the sprayed region, i.e. as long as θ is less than γ. Otherwise, the thickness increase rate is zero. As vacuum filtration does not affect the solid particle mass increase rate, dm_p can only increase or remain constant over time.

To find $d\dot{m}_w$, combine Equations (2.1.5), (2.2.2), (2.2.9), and (2.2.20) and take a time derivative.

$$dm_w = (1-s) \int_{t_0}^{t_f} C_D C_I dAH(\gamma - \theta) dt - \frac{\rho_w \Delta P dA}{\mu} \int_{t_0}^{t_f} \left[\frac{c^{1+\tau}}{C_k} \delta + C_F \frac{\Delta P}{\mu_w} \right]^{-1} dt \tag{2.3.3}$$

$$d\dot{m}_w = (1-s) C_D C_I dAH(\gamma - \theta) - \frac{\rho_w \Delta P dA}{\mu} \left[\frac{c^{1+\tau}}{C_k} \delta + C_F \frac{\Delta P}{\mu_w} \right]^{-1} \tag{2.3.4}$$

Before using Equation (2.3.4), a small modification must be made. Consider the case where there is no water mass present in a differential area dA, either because no mass has been sprayed on this point or all of the water mass has been filtered out. Equation (2.3.4) is then modified to include the same step function used in Equation (2.1.3) to remove the effects of vacuum filtration to account for these two cases.

$$d\dot{m}_w = (1-s)C_D C_I dAH(\gamma-\theta) - \frac{\rho_w \Delta P dA}{\mu}\left[\frac{c^{1+\tau}}{C_k}\delta + C_F\frac{\Delta P}{\mu_w}\right]^{-1} H(dm_w) \tag{2.3.5}$$

The water mass increase rate due to the spray process is constant as long as the differential area dA is within the sprayed region. Otherwise, the water mass increase rate is zero. The water mass decrease rate due to vacuum filtration is not constant, and varies with δ and c. As δ and c increase, the rate of water filtration decreases, and vice versa.

To find $\dot{\delta}$, begin by combining Equations (2.1.5) and (2.2.1), taking a time derivative, removing the common dA term, and then solving for the resulting $c\dot{\delta}$ term.

$$c\rho_p \delta dA = s\int_{t_0}^{t_f} C_D C_I dAH(\gamma-\theta)\ dt \tag{2.3.6}$$

$$\rho_p(\dot{c}\delta + c\dot{\delta}) = sC_D C_I dAH(\gamma-\theta) \tag{2.3.7}$$

$$c\dot{\delta} = \frac{s}{\rho_p}C_D C_I dAH(\gamma-\theta) - c\dot{\delta} \tag{2.3.8}$$

Now, combine Equations (2.1.5), (2.2.2), (2.2.9), and (2.2.20), take a time derivative, and remove the common dA term.

$$(1-c)\rho_w \delta dA = (1-s)\int_{t_0}^{t_f} C_D C_I dAH(\gamma-\theta)\ dt - \frac{\rho_w \Delta P dA}{\mu}\int_{t_0}^{t_f}\left[\frac{c^{1+\tau}}{C_k}\delta + C_F\frac{\Delta P}{\mu_w}\right]^{-1} dt \tag{2.3.9}$$

$$(1-c)\dot{\delta} - \dot{c}\delta = \frac{(1-s)}{\rho_w} C_D C_I dAH(\gamma-\theta) - \frac{\rho_w \Delta P dA}{\mu}\left[\frac{c^{1+\tau}}{C_k}\delta + C_F\frac{\Delta P}{\mu_w}\right]^{-1} \tag{2.3.10}$$

Finally, insert Equation (2.3.8) into Equation (2.3.10) and solve for $\dot{\delta}$

$$(1-c)\dot{\delta} - \frac{s}{\rho_p} C_D C_I dAH(\gamma-\theta) + c\dot{\delta} = \frac{(1-s)}{\rho_w} C_D C_I dAH(\gamma-\theta) - \frac{\rho_w \Delta P dA}{\mu}\left[\frac{c^{1+\tau}}{C_k}\delta + C_F\frac{\Delta P}{\mu_w}\right]^{-1} \tag{2.3.11}$$

$$\dot{\delta} = \left[\frac{s}{\rho_p} + \frac{(1-s)}{\rho_w}\right] C_D C_I dAH(\gamma-\theta) - \frac{\rho_w \Delta P dA}{\mu}\left[\frac{c^{1+\tau}}{C_k}\delta + C_F\frac{\Delta P}{\mu_w}\right]^{-1} \tag{2.3.12}$$

Again, however, the case where $d\dot{m}_w$ is 0 must be considered. In this case, the decrease in δ due to filtration does not go to zero. This is again incorrect as it can lead to filter cakes with negative thicknesses. The same step function used in Equation (2.1.3) must then be included to cancel out the effects of vacuum filtration when no water mass is present.

$$\dot{\delta} = \left[\frac{s}{\rho_p} + \frac{(1-s)}{\rho_w}\right] C_D C_I dAH(\gamma-\theta) - \frac{\rho_w \Delta P dA}{\mu}\left[\frac{c^{1+\tau}}{C_k}\delta + C_F\frac{\Delta P}{\mu_w}\right]^{-1} H(dm_w) \tag{2.3.13}$$

Equation (2.3.13) is the differential equation for the thickness of the filter cake δ in a differential area dA with respect to time. Equation (2.3.13) has two main parts: an increase due to the spray nozzle, and a decrease due to vacuum filtration.

The thickness increase rate due to the spray process is constant as long as the differential area dA is within the sprayed region. Otherwise, this thickness increase rate is zero.

The thickness decrease rate due to vacuum filtration is not constant, and varies with δ and c.

As the thickness can only increase as solid particles and water are deposited by the spray process, δ can only increase as both dm_p and dm_w increase. Similarly, as the thickness can only decrease as water is removed by filtration, δ can only decrease as dm_w decreases.

The concentration increases as water is removed by vacuum filtration, but decreases as solid particles and water are deposited by the spray process. It follows that as c decreases, δ will increase, and vice versa. Smaller, less concentrated filter cakes experience quick filtration. Thicker, more concentrated filter cakes experience much slower filtration.

If a spray is applied to a differential area dA for a finite amount of time while vacuum pressure is applied for an infinite amount of time, dm_p will reach a constant final value while dm_w will go to 0. The final value for dm_p can be calculated by multiplying Equation (2.3.2) by the time the differential area dA stays within the spray, denoted by t_s, and by removing the step function.

$$dm_{p,f} = sC_D C_I dA t_s \tag{2.3.14}$$

Here $dm_{p,f}$ is the final mass of the solid particulate in a differential area dA. It also follows that δ will reach a steady state condition once dm_w reaches 0. At this point, δ_f, the final thickness, is determined by $dm_{p,f}$. It then holds that δ_f is determined by the amount of time dA is sprayed. Longer sprays will yield thicker filter cakes, while shorter sprays will

yield smaller filter cakes. δ_f can be approximated from Equations (2.2.1) and (2.3.14), and by noting that the final c is 1 as

$$dm_{p,f} = sC_D C_I dAt_s = \rho_p \delta_f dA \tag{2.3.15}$$

$$\delta_f = \frac{sC_D C_I dAt_s}{\rho_p} \tag{2.3.16}$$

CHAPTER 3

PARAMETER ESTIMATION

3.1 Experiment Procedure

There are four unknown parameters in Equations (2.3.2), (2.3.5), and (2.3.13) that must be defined: C_D, C_F, C_k, and τ. The experiment setup is shown in Figure 3.1, and the experiment procedure for identifying these values is as follows: A strip of filter paper is weighed and placed between a moveable spray nozzle and a vacuum filter. Vacuum pressure is then applied to the filter paper and a mixture of water and solid particles is sprayed onto the filter paper. During the spray period, the nozzle moves across the length of the filter paper. Once the nozzle has reached the end of the filter paper, the spray is stopped, and the vacuum pressure remains on for a set period. This extra filter time is varied between experiments. The filter paper is then re-massed, and the change in mass is calculated. A two-loop nonlinear constrained optimization algorithm, to be discussed in Section 3.2, is applied to determine the unknown constants based off the mass change.

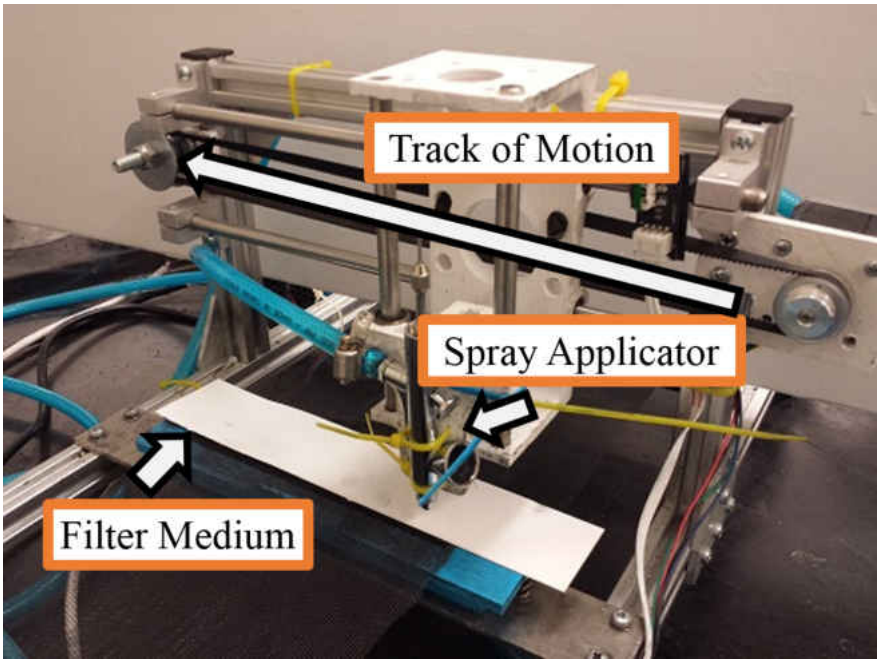

Figure 3.1: Experiment Setup

In this study, sheets of carbon nanofiber embedded paper are created. The mixture used contains 150 mL of water and 1.5 g of carbon nanofibers. In all cases, the following values are used: ΔP is 27 inHg, ρ_p is 1500 kg/m3, A_s is 0.126 mm2, ΔP_s is 20 psi, z_a is 5 mm, and γ is 9deg. The path the nozzle takes in each case is 10 cm long, and is completed in 4.2 seconds.

Equation (2.3.16) can be used to predict the final thickness at a point in terms of C_D. For a linear path, the maximum spray time a point can experience can be found by dividing the diameter of the sprayed region by the speed of the applicator. In this case, the spray time is 0.0654 s. From this, the predicted is about 0.1145 C_D mm.

3.2 Identification Algorithm

Several different methods can be used to identify unknown parameters within a model. In this paper, an identification scheme using a nested loop of two nonlinear constrained optimizations, similar to that used in [20], is used to find values for C_D, C_F, C_k, and τ. An inner loop chooses values for the unknown terms, and then simulates the filtration process, while an outer loop chooses boundaries for the inner loop to ensure the identified values converge with one another. The simulations are performed on a laptop with 8.00 GB of RAM, an i7-4510U CPU, and Ubuntu 14.04 LTS for the operating system. The identification scheme is run using Matlab R2013a, and Matlabs fmincon function is used for both the inner and outer loops. A simple Euler scheme is used for integration, with a time step of 0.01 s and a differential area of 0.01 mm2. The concentration of the filter cake within a differential area is calculated using Equation (2.2.1).

In this simulation, the filter paper is broken into many small differential areas dA, and the nozzle follows the path described in the experiment setup. At each time step, $d\dot{m}_p$, $d\dot{m}_w$, and $\dot{\delta}$ are calculated and integrated at each dA according to Equations (2.3.2), (2.3.5), and (2.3.13). Once the nozzle has reached the end of its path, $d\dot{m}_p$ is set to 0 and the effects of the spray process are removed from $d\dot{m}_w$ and $\dot{\delta}$ at all points for the remainder of the simulation. If dm_w reaches 0 within a differential area dA, then no further water can be removed from this point, and $d\dot{m}_w$ and $\dot{\delta}$ are set to 0 at this point for the remainder of the simulation. At the end of the extra filter time, dm_p and dm_w are integrated across the

entire surface of the filter paper, and the following performance index is then calculated for experiment i as

$$J_{in,i} = \left| \frac{m_{p,i} + m_{w,i} - \Delta m_i}{\Delta m_i} \right| \tag{3.2.1}$$

Here $m_{p,i}$ is the mass of the solid particles at the end of the simulation for experiment i, $m_{w,i}$ is the mass of the water at the end of the simulation for experiment i, and Δm_i is the measured increase of the mass of the filter paper in experiment i. The inner loop is iterated such that the unknown parameters C_D, C_F, C_k, and τ are selected to minimize $J_{in,i}$.

The values chosen in the inner loop are constrained by upper and lower bounds, which are determined by an outer loop. This outer loop is necessary to ensure that the identified parameters from each experiment agree well with each other, as there are many local minima that the inner loop can settle on. The outer loop cost function J_out is defined as.

$$J_{out} = \frac{\sigma_{C_D}}{X_{C_D}} + \frac{\sigma_{C_F}}{X_{C_F}} + \frac{\sigma_{C_k}}{X_{C_k}} + \frac{\sigma_\tau}{X_\tau} + \sum P_i \tag{3.2.2}$$

Here the σ terms are the standard deviations of the parameters found by the inner loop, the X terms are the maximum values of the parameters found by the inner loop, and P_i is a penalty imposed when $J_{in,i}$ is above a user-defined threshold. The bounds chosen by the outer loop are themselves bounded by upper and lower bounds. Additionally, the bounds chosen for the inner loop must be separated by an amount which must be within a user defined range.

In order to use this identification scheme, an initial guess and initial bounds for the outer loop variables must be supplied. Unlike in [20], there were no known expected values or ranges for the unknown parameters. Instead, it was observed that the Δm for Experiments 3 and 4 were very similar. Because of this similarity, it was assumed that the filter cake created in Experiment 3 still had some water remaining, while the filter cake created in Experiment 4 had all of its water removed. To find an initial guess, values for C_D and C_F were manually chosen until J_{in} for both Experiments 3 and 4 was below 0.10. This process was then repeated for all four experiments with all four unknown parameters until for each experiment was below 0.10. The initial guess for the outer loop was then set to be 10% above and below the manually identified values. The outer loop bounds were then set to be 25% above and below the manually identified values, centering on the manually identified values. The algorithm of the identification scheme is shown in Table 3.1.

Table 3.1: Algorithm Table

Step 1	Supply the initial guess of the parameter bounds to the outer loop
Step 2	Set the initial guess of the parameters for the inner loop equal to the mean of the current outer loop guess
Step 3	Set the inner loop bound equal to the current outer loop guess
Step 4	Simulate the filtration process using the current inner loop guesses for C_D, C_F, C_k, and τ
Step 5	Calculate $J_{in,i}$
Step 6	Vary inner loop guess, and repeat Steps 4 and 5 until $J_{in,i}$ is minimized
Step 7	Repeat Steps 4, 5, and 6 for all 4 experiments
Step 8	Calculate J_{out}
Step 9	Vary the outer loop guess, and repeat Steps 2 through 8 until J_{out} is minimized

3.3 Experiment Results

The results of four experiments conducted are shown in Table 3.2. In each case it was observed that as the filter time increased, the change in mass decreased.

The values identified using the previously discussed outer loop guess and outer loop bounds, along with the simulated masses and inner loop costs, can be seen in Table III. It can be seen from Table III that the identified values produce masses that are close to those measured. As expected, the simulations for each experiment produce similar values for m_p, while m_w goes to 0 as the filter time increases. J_{out} for the identified parameters is 0.0255, indicating that the identified results agree well for all experiments. The average maximum simulated final thickness in areas that had been completely dewatered was 0.221 mm, which matches well with the predicted final thickness of 0.220 mm using the average identified value for c_D.

Table 3.2: Experiment Results

Experiment	Spray Time (s)	Extra Filter Time (s)	Increase in mass (g)
1	4.2	2.95	0.1097
2	4.2	3.50	0.0606
3	4.2	3.90	0.0449
4	4.2	4.35	0.0420

Table 3.3: Identification Results

Unknown Parameter	C_D	C_F (s/m)	C_k (m^2)	τ
Average Estimated Value	1.9194	122.1	5.050e-13	10.50
Estimated Value Range	1.9029 - 1.9525	120.0 - 124.0	5.049e-13 - 5.050e-13	10.49 - 10.50
Experiment	1	2	3	4
m_p (g)	0.04128	0.04105	0.04119	0.04202
m_w (g)	0.06877	0.01955	0.00373	0.00000
J_{in}	1.282e-5	1.607e-6	3.933e-8	1.196e-5

The 3D nanoparticle layer thickness plots for the simulated manufacturing process at various points in time are show in Figures 3.2 through 3.7. The simulations used for these figures were performed using the average identified values in Table 3.3, with a time step of 0.001 s and a differential area of 0.0025 mm^2. As the simulated nozzle follows the path described in the experiment procedure, areas closer to the beginning of the paper experience both spray and vacuum filtration before those areas closer to the end of the path. This manifests in the simulation as an elevated area that moves from the beginning to the end of the paper, with areas that have not yet experienced spray and areas that have been completely dewatered appearing identical. The apparent magnitude of this elevated area when compared to the areas before and after it can be explained by noting that the mass fraction of the carbon nanofibers in the spray is very small, and that the main component of this area is water. The final thickness, which is entirely due to the nanofibers, is much smaller than the maximum thickness increase that occurs during spray. Once the nanopaper has been completely dewatered, its thickness is constant along the length of the paper but varies with the papers width. This is expected, as the sprayed area is circular, and those differential areas further away from the nozzle experience less spray time.

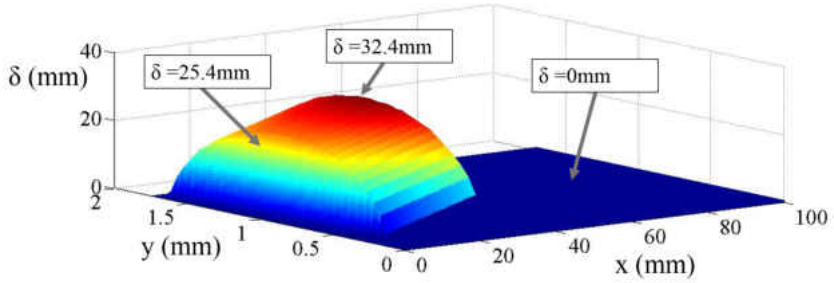

Figure 3.2: Thickness profile after 1 s of spray

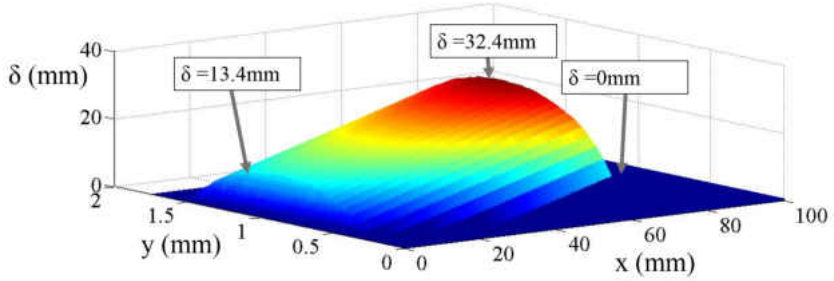

Figure 3.3: Thickness profile after 2.5 s of spray

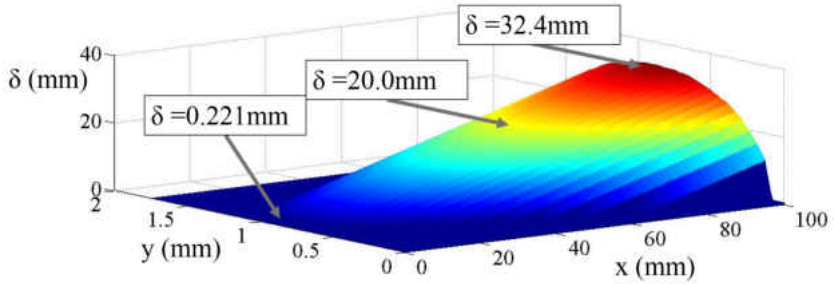

Figure 3.4: Thickness profile after 4.2 s of spray

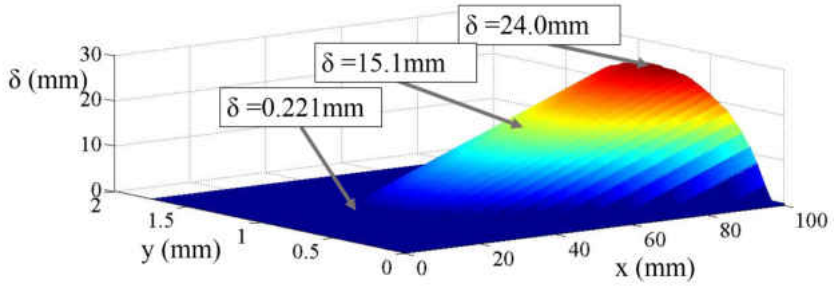

Figure 3.5: Thickness profile after 1 s of filtration

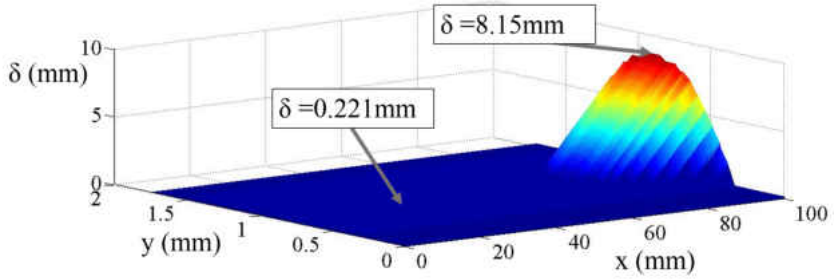

Figure 3.6: Thickness profile after 3 s of filtration

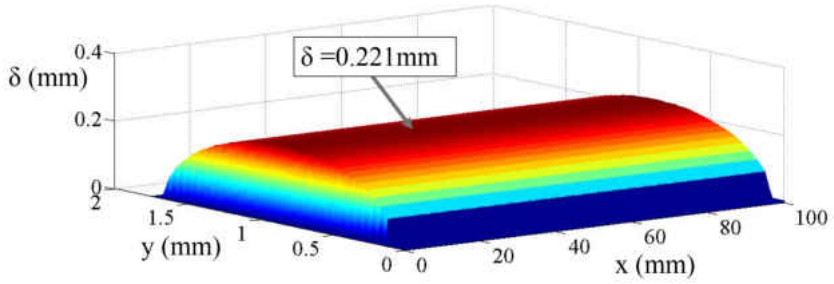

Figure 3.7: Thickness profile after 4.5 s of filtration

CHAPTER 4

CONCLUSIONS AND FUTURE WORK

A discussion on a thickness model for filter cakes created through spray-assisted vacuum filtration has been presented. The mass transfer dynamics from spray atomization and vacuum filtration are studied, and state space model for the spray assisted vacuum filtration process has been developed. An identification scheme for any unknown terms in the model has been developed. A method for calculating the permeability based off of concentration has been introduced. An expression for the final thickness based off of the spray trajectory has been derived.

4.1 Future Work

In the future, this model can be used to enable precision thickness control of nanoparticle sheets made using spray assisted vacuum filtration. The model can be used to generate path planning algorithms for a spray applicator, enabling a user to create specific thickness profiles.

LIST OF REFERENCES

[1] A. Arsha, T. Jayakumar, E.and Rajan, V. Antony, and B. Pai, "Design and fabrication of functionally graded in-situ aluminium composites for automotive pistons," *Compos. Struct.*, 2015.

[2] C. Soutis, "Fibre reinforced composites in aircraft construction," *Prog. Aerospace Sci.*, 2005.

[3] Y. Wang and O. Zhupanska, "Lightning strike thermal damage model for glass fiber reinforced polymer matrix composites and its application to wind turbine blades," *Compos. Struct*, 2015.

[4] G. Mittal, V. Dhand, K. Rhee, S. Park, and W. Lee, "A review on carbon nanotubes and graphene as fillers in reinforced polymer nanocomposites," *J. Ind. Eng. Chem.*, 2015.

[5] M. Shahadat, T. Teng, M. Rafatullah, and M. Arshad, "Titanium-based nanocomposite materials: A review of recent advances and perspectives," *Colloids Surf., B*, 2015.

[6] A. Rushton, A. Ward, and R. Holdich, *Solid-Liquid Filtration and Separation Technology*, ch. 2. Wiley, 2000.

[7] S. Seriani, A. Cortellessa, S. Belfio, M. Sortino, G. Totis, and P. Gallina, "Automatic path-planning algorithm for realistic decorative robotic painting," *Automat. Constr.*, 2015.

[8] Z. Liu, W. Zhang, J. Ouyang, and Y. Zhou, "Novel thermal barrier coatings based on rare-earth zirconates/ysz double-ceramic-layer system deposited by plasma spraying," *J. Alloy Compd.*, 2015.

[9] F. Aziz and A. Ismail, "Spray coating methods for polymer solar cells fabrication: A review," *Mat. Sci. Semicon. Proc.*, 2015.

[10] N. Pham, J. Burghartz, and P. Sarro, "A model for film thickness using direct spray coating," in *Proc. 2003 Electron. Packag. Technol.*, 2003.

[11] M. True, "Modeling of electrostatic spray plumes," *IEEE Trans. Ind. Appl.*, 1983.

[12] M. Li, D. Shi, and P. Christofides, "Modeling and control of an experimental hvof thermal spray process," in *Proc. 2003 American Control Conference*, 2003.

[13] A. Bejan, *Heat Transfer*. Wiley, 1993.

[14] S. Duncan, "A frequency-domain approach to determining the path separation for spray coating," *IEEE Trans. Autom. Sci. Eng.*, 2005.

[15] X. Huang, Q. Zhou, L. Zeng, and X. Li, "Monitoring spatial uniformity of particle distributions in manufacturing processes using the k function." accepted and in print.

[16] A. Lefebvre, *Atomization and Sprays*. Hemisphere Publ. Corp., 1989.

[17] S. Suh, I. Woo, and S. Noh, "Development of an automatic trajectory planning system (atps) for spray painting robots," in *Proc. 1991 IEEE Int. Conf. Robotics and Automation*, 1991.

[18] D. Conner, A. Greenfield, P. Atkar, A. Rizzi, and H. Choset, "Paint deposition modeling for trajectory planning on automotive surfaces," *IEEE Trans. Autom. Sci. Eng.*, 2005.

[19] P. Hertling, L. Hog, R. Larsen, J. Perram, and H. Petersen, "Task curve planning for painting robots part i: process modeling and calibration," *IEEE Trans. Robot. Autom.*, 1996.

[20] H. Shen, A. Mark, K. Thompson, Y. Xu, F. Liang, J. Gou, and B. Mabbott, "Thermal modeling and cofficient identification of shape memory polymer nanocomposites structure," *Appl. Phys. Lett.*, 2015.